A major purpose of the Technical Information Center is to provide the broadest dissemination possible of information contained in DOE's Research and Development Reports to business, industry, the academic community, and federal, state and local governments.

Although a small portion of this report is not reproducible, it is being made available to expedite the availability of information on the research discussed herein.

LA-UR -87-83

LA-UR--87-83

DE87 005113

Los Alamos National Laboratory is operated by the University of California for the United States Department of Energy under contract W-7405-ENG-36

TITLE PLASMA ENERGY BALANCE MODEL FOR OPTICAL-LASER-INDUCED IMPULSE

AUTHOR(S): R. S. Dingus, X-DOT
S. R. Goldman, X-1

SUBMITTED TO Int'l Conf. on Lasers '86
Orlando, FL
Nov. 3-7, 1986

DISCLAIMER

Los Alamos National Laboratory
Los Alamos, New Mexico 87545

LA-UR-87-83

000705

PLASMA ENERGY BALANCE MODEL FOR OPTICAL-LASER-INDUCED IMPULSE IN VACUO

R. S. Dingus and S. R. Goldman

Los Alamos National Laboratory, Los Alamos, NM 87545

Abstract

A simple plasma-energy-balance model, along with its derivation, is presented for calculating the impulse from targets in a vacuum exposed to single-pulse, optical lasers. Figures demonstrate that throughout most of the range of interest, results from the model agree well with experimental data and LASNEX radiation-hydrodynamic computer code calculations. The model assumes isothermal blowoff and thus takes advantage of the insensitivity of impulse to energy distribution within the ablated mass. The density profile in the blowoff plasma is estimated and the Saha equation is used to evaluate the degree of ionization. The laser absorption coefficient and thermal radiation opacity are evaluated as a function of position in the plasma in order to evaluate the energy reaching the ablation surface. An overall energy balance plus an energy balance at the ablation surface are used to determine the blowoff mass and temperature. The success of the model indicates that the impulse is insensitive to detailed interactions in the vicinity of the ablation surface.

I. Introduction

The momentum per unit area induced by lasers incident on targets in a vacuum is a function the photon wavelength; the flux (intensity) as a function of time; the fluence (integral of flux over time), the angle of incidence; the beam diameter (unless it is sufficiently large); and the target's material and geometric properties. In this paper, the target is assumed to be flat, the beam incident normal to the surface, and the beam diameter sufficiently large that the blowoff is one dimensional (i.e., that gradients in the blowoff such as temperature, density, etc. only exist in the direction normal to the target surface). The region of emphasis for this paper is from the threshold for impulse up to a flux of about 10^{16} W/m^2 or to a fluence of about 10^{10} J/m^2.

Reference 1 discuses the phenomenology of optical-laser-induced impulse in vacuo and developes a model, based upon overall energy balance, for calculating impulse in which the mass loss is allowed to be a free parameter. In this paper, another equation based upon energy balance at the ablation surface is developed and added to that model, thus fixing the mass loss and allowing impulse predictions to be obtained without a posteriori knowledge of the blowoff mass.

Results from this model, which will be referred to here as the plasma-energy-balance model, agree well with both experimental data and LASNEX hydrodynamic computer-code calculations, although one-dimensional data do not exist at high fluences. Although, in the development of the model, considerable attention is given to evaluating the energy transfer through the blowoff to the ablation surface, little attention (other than enthalpy considerations) is given to the complicated thermodynamics at the ablation surface. The success of the model indicates that the impulse is insensitive to detailed interactions in the vicinity of the ablation surface. This is fortunate because these interactions are not easy to assess accurately because of the large temperature, density, etc. gradients in this region.

II. Plasma-Energy-Balance Model

A. Basic Model

The model is described by a set of self-consistent equations summarized in the Appendix B. The symbols used in the equations are defined in Appendix A. Most of these equations were developed in Ref. 1. They are discussed briefly in this section; more detail can be obtained from Ref. 1. Details regarding derivation of the energy balance equations are presented in Section II b. They rely upon the fact (shown in Ref. 1) that the impulse is insensitive to the distribution of kinetic energy within the blowoff mass. If the total blowoff mass and energy within are known, along with a rough approximation of the distribution of energy within the mass, then the impulse can be predicted accurately.

Following that lead, the model is based upon the assumption that, for any given laser pulse incident on a target, the blowoff will be isothermal with temperature T. The blowoff particles are assumed to have a Maxwell-Boltzmann

distribution of velocities with an average velocity <v> given by

$$\langle v\rangle = \{[8/\pi]N_0 kT/\langle A\rangle\}^{1/2}, \quad \langle A\rangle = A/(1+Z) \quad . \tag{1}$$

Further, it is assumed that the laser flux Φ_0 and the mass ablation rate dm/dt are constant during the laser pulse and that no ablation occurs after the pulse. These assumptions have been made for simplicity to allow a simple time-integrated solution to the problem. However, it appears that other temporal functions for the flux and ablation rate could also be used. Better yet, but with considerable increase in model complexity, a time-dependent solution with this basic model for an arbitrary temporal profile for the flux should be possible by solving the rate equations for the ablation rate (instead of first integrating them over time) and then stepping through time. Further, it appears that the model could be extended to include two-dimensional effects for cases where, during the laser pulse, the blowoff traverses distances large compared to the laser beam diameter.

Using these assumptions, plus the assumption that there is no interaction between the particles in the blowoff, allows an equation to be derived[1] for the density ρ as a function of position z within the blowoff

$$\rho/\rho_0 = \exp(-\zeta^2) \ , \quad \rho_0 = [4/\pi][dm/dt]/\langle v\rangle \ , \quad \zeta \equiv z/z_0 \ , \quad z_0 = [\pi/4]\langle v\rangle \tau \ ,$$
$$m/M = \mathrm{erf}(\zeta) \ , \quad m = m(z) = \int_0^z \rho(z')\,dz' \ , \quad M = m(\infty) \ , \quad \mu \equiv 1 - m/M \quad . \tag{2}$$

For $\zeta > 2$, these equations can be combined to give

$$\rho/\rho_0 = \mu \quad . \tag{3}$$

The quantity μ has the value one at the ablation surface and zero at infinity. It represents the fractional mass thickness of the blowoff, from the outside in, to a mass distance m from the ablation surface. Studies of ion rarefaction waves in plane geometry have given similar expressions for the density profile.[2,3]

The degree of ionization Z of the blowoff is obtained from an approximate solution of the Saha equation using the approach by Zel'dovich and Raizer,[4] which assumes the ionization levels I_Z are a continuous, rather than discrete function of Z:

$$Z = [2/n_0][2\pi m_e kT/h^2]^{3/2} \exp(-\langle I_Z\rangle/kT), \quad n_0 = \rho_0 N_0/A \ , \quad n_{eo} = Z\, n_0 \quad . \tag{4}$$

For simplicity, the ionization value used throughout the blowoff is calculated using the density at the ablation surface. Ionization levels calculated by Cowan[5] are available for use in this equation. Using Kramer's formula corrected for induced emissions for the inverse bremsstrahlung cross section, expressed in units of area per unit mass,

$$\kappa^L_0 = [4/3]\{2\pi/[3kT]\}^{1/2}[N_0/A]^2\{\rho Z^3 e^6/[hcm_e^{3/2}\nu^3]\}\{1-\exp(-h\nu/[kT])\} \ , \quad \kappa^L(\mu) = \mu\,\kappa^L_0 \ , \tag{5}$$

expressions (derived in the next section of this paper) are obtained for the location μ_L of peak laser absorption in the blowoff

$$\mu_L = [\kappa^L_0 M]^{-1/2} \quad \text{for} \quad [\kappa^L_0 M]^{-1/2} \le 1 \ ,$$
$$= 1 \quad \text{for} \quad [\kappa^L_0 M]^{-1/2} > 1 \ , \tag{6}$$

the linear distance of the laser absorption plane, z_L, from the ablation surface (using Eqs. 2, 3, and 6)

$$z_L = z_0\,|\ln \mu_L^{-1}|^{1/2} \ , \tag{7}$$

and the fraction ε_L of laser penetration to the ablation surface

$$\varepsilon_L = [1-\exp(-I^L_M)]/I^L_M \ , \quad I^L_M = 0.5\, M\, \kappa^L_0 \ . \tag{8}$$

The quantity l^L_M is the thickness of the blowoff to the laser photons expressed in number of mean free paths.

Similarly, the location μ_c (or z_c) of the critical surface is

$$\mu_c = \rho_c/\rho_o = n_{ec}/n_{eo} \quad \text{for} \quad n_{ec}/n_{eo} \le 1 \quad , \qquad n_{ec} = \pi m_e c^2/(e^2\lambda^2) \quad ,$$
$$= 1 \qquad\qquad\qquad \text{for} \quad n_{ec}/n_{eo} > 1 \quad ,$$

$$z_c = z_o [\ln \mu_c^{-1}]^{1/2} \quad . \tag{9}$$

For the region of interest here, calculations with this model indicate that nearly all laser photons are absorbed by inverse bremsstrahlung before reaching the critical surface. When the degree of ionization Z becomes small, Kramer's formula for the inverse bremsstrahlung cross section gives values less than the real cross section. The model ignores the Gaunt factor (i.e., assumes it to be 1) in the inverse bremsstrahlung cross section for the following reasons: the factor is normally about 1, except near the critical surface; the critical surface is treated separately and does not normally exist in the blowoff anyway; inclusion of the Gaunt factor interfers with scaling of the absorption coefficient with density.

Figure 3 of Ref. 1 presents the Rosseland mean opacity from the SESAME Equation of State Library[3] for aluminum as a function of temperature and density. Examination of this figure shows that the Rosseland mean opacity κ^R_{Al} for aluminum over the range of temperatures and densities of interest to this work can be approximated by

$$\kappa^R_{Al}(m^2/kg) = 6 \times 10^4 \, T(eV)^{-2} \, \rho(kg/m^3), \quad \kappa^R(\mu) = \mu \, \kappa^R_o \quad . \tag{10}$$

As in the case of the inverse bremsstrahlung absorption coefficient, this Rosseland mean opacity for the thermal radiation is approximately proportional to ρ so that the opacity at position μ is approximately μ times κ^R_o, the Rosseland mean opacity at the ablation surface. In some regions, values from Eq. 10 differ significantly from the tables; for more accurate modeling in a particular region of interest, a relation normalized to the tables in that region would be more appropriate. Similarly, using tabular values for the laser absorption coefficient instead of Eq. 5 might improve the accuracy of calculations in certain regions; however, the results from the model generally seem to be insensitivity to the values for the laser absorption coefficients and thermal radiation opacities used.

Assuming that the location of peak laser absorption is the principal source region for thermal radiation in the blowoff, and using Eq. 10 for the Rosseland mean opacity, expressions are obtained for the fraction ε_i (i implies "in") of thermal radiation reaching the ablation surface

$$\varepsilon_i = \mu_L^2 + [1 - \exp(-l^R_M[1-\mu_L^2])]/l^R_M \quad , \qquad l^R_M = 0.5 \, M \, \kappa^R_o \quad , \tag{11}$$

and for the fraction ε_o (o implies "out") lost into the vacuum

$$\varepsilon_o = \mu_L^2 \, [1 - \exp(-r_{RL})]/r_{RL} + [1-\mu_L^2] \exp(-r_{RL}) \quad , \qquad r_{RL} = 0.5 \, \kappa^R_o/\kappa^L_o \quad . \tag{12}$$

Using the above expressions, two flux balance equations based upon conservation of energy are assumed to hold. These two equations are integrated over time to yield energy balance equations; one is an overall energy balance; the other is an energy balance at the ablation surface. Energy transport by monochromatic laser radiation and by thermal radiation are considered; electron conduction in the blowoff is ignored. Conduction in the blowoff does not appear to be significant in the region of interest in this paper. Attenuation of both the laser and thermal radiation by the blowoff is included.

The overall balance equates the laser energy absorbed $\alpha' F_o$ to the energy absorbed by the target F_a plus the energy radiated into the vacuum

$$\alpha' F_o = F_a + \varepsilon_o \sigma T^4 \tau \quad , \quad \alpha' = 1 - (1-\alpha) \, \varepsilon_L' \quad , \qquad \varepsilon_L' = [1-\exp(-2 \, l^L_M)] \, / \, [2 \, l^L_M] \quad . \tag{13}$$

The laser energy absorbed is taken to be the incident fluence F_o times α' where α' includes consideration of reflection

R (= 1-α) at the ablation surface surface and attenuation ε_L' of the laser photons on the way in and back out of the plasma. The reflectivity is not predicted by the model and therefore must be obtained from other sources; its value can be near 1 for certain cases; however, at high flux ε_L' approaches zero and thus α' approaches 1 at high flux. The energy absorbed by the target is assumed to equal the energy conducted into the solid, the energy to vaporize and ionize the blowoff, plus the thermal kinetic energy of the blowoff

$$F_a = [\{4/\pi\}K c_p \rho \tau]^{1/2} T_s + M[\Delta H + \{N_0/A\} \Sigma I_Z + \{3/2\}N_0 kT/<A>] \quad . \tag{14}$$

Radiation energy within the blowoff is ignored and no distinction is made between thermal and translational kinetic energy. The balance at the ablation surface equates the energy reaching the ablation surface with that absorbed by the target

$$\varepsilon_L \alpha F_0 + \varepsilon_i \sigma T^4 \tau = F_a \quad . \tag{15}$$

All of the above equations are written parametrically in terms of temperature. As discussed below, a self-consistent solution can be found by iteration that determines the blowoff mass and laser fluence absorbed for any given temperature.

The (specific) impulse (momentum per unit area integrated over all time) is obtained by multiplying the blowoff mass M times the average blowoff velocity <v> times a geometric factor G

$$I(\infty) = G M <v> \tag{16}$$

The geometric factor is included in the equation for the impulse to account for the directionality of the blowoff; if all blowoff is directed normal to the surface, this factor is equal to 1; if the blowoff is isotropic into 2π solid angle away from the blowoff surface, this factor is equal to 1/2. Experiments generally tend to indicate that this factor is near 1.

From the density and temperature, the pressure at the ablation surface can be calculated

$$p_0(t \le \tau) = G n_0 [1 + Z] kT \quad . \tag{17}$$

Because of the assumptions of constant temperature and mass ablation rate, this calculated pressure is constant during the laser pulse. Multiplying this pressure by the pulse length gives an impulse that is equal to 1/2 of the total impulse calculated above using the blowoff mass

$$I(\tau) = [1/2] G M <v> = p_0 \tau \quad . \tag{18}$$

Assuming that the pressure decays exponentially after the laser pulse ends and that the other half of the impulse is imparted during the pressure decay after the pulse, then the time constant for this decay is equal to the laser pulse length, that is

$$p_0(t \ge \tau) = G n_0 [1 + Z] kT \exp(-[t - \tau]/\tau) \quad . \tag{19}$$

B. Energy Balance

In this section, expressions are developed for the energy flux onto the ablation surface as well as the energy lost back into the vacuum. These expressions are then used in equations for energy balance described in the previous section.

Attenuation of the thermal radiation is estimated by finding the location of peak energy deposition of the laser photons and assuming this is a hot plane in the blowoff cloud (as a perturbation to the assumption of constant temperature in the blowoff). The hot plane is assumed to radiate a flux of σT^4, both inward and outward. Assumed emission from this single plane is reasonable because of the strong T^4 factor. The assumed emission rate (σT^4) is an

upper limit and the actual rate could be substantially smaller if this region was optically thin to the thermal radiation. It is not clear how an error of this nature would affect the impulse because there are compensating factors; more emission increases the mass loss and the impulse, but it also increases energy loss into the vacuum, which decreases the impulse. Given the emission plane, attenuation of the thermal radiation is obtained using an approximate expression for the Rosseland mean opacity.

Calculations with this model, as well as with LASNEX, show that, for the region of interest here, the laser photons are nearly all absorbed in the blowoff before reaching the critical surface except very early in the pulse. For times when the energy density does not reach a maximum in the blowoff, the hot plane is taken to be the ablation surface.

A photon flux Φ is attenuated by a mass (per unit area) increment dm with cross section κ (area per unit mass) by an amount specified by

$$d\Phi/\Phi = -\kappa\, dm \quad . \tag{20}$$

Integrating this equation over the blowoff into the position μ gives the flux at position μ as

$$\Phi(\mu) = \Phi_0 \exp(-{}^{L}\kappa_M\, \mu^2) \quad . \tag{21}$$

The location of the hot plane can be found in the following manner. The energy density $\xi(\mu)$ (per unit mass) can be found by taking the derivative of Eq. 21 with respect to mass depth m giving

$$\xi(\mu) = {}^{L}\kappa_0\, \mu\, \Phi(\mu) \quad . \tag{22}$$

In Eq. 22, laser absorption in the plasma of photons reflected from the ablation surface are ignored because we are locating the hot plane that occurs when the photons are all absorbed before reaching the ablation surface. Taking the derivative of Eq. 22 with respect to mass and setting it equal to zero and solving for μ ($\equiv \mu_L$; L $\Rightarrow$ laser absorption plane) gives the location of the maximum energy density as given above in Eq. 6. For constant ablation rate ($dm/dt = M_\tau/\tau$), the condition on Eq. 6 implies that the peak energy density is at the ablation surface for a time t_0 given by

$$t_0 = [\, {}^{L}\kappa_0\, dm/dt\,]^{-1} \quad . \tag{23}$$

When the free electron density for the blowoff at the ablation surface n_{e0} is greater than the critical electron density n_{ec}, then there is a critical surface in the blowoff at the location where thie ratio of these electron densities equals one. Since the model assumes that Z is constant in the blowoff, the location of the critical surface μ_c is obtained by setting this ratio equal to the mass density ratio as in Eq. 9.

Assuming constant ablation rate, Eqs. 6 and 9 show that μ_c has a fixed value independent of time but that μ_L decreases with time because M is proportional to time ($M = [dm/dt]\, t$ for $t \le \tau$). Also, at the beginning of the pulse, μ_L always equals 1 (i.e., the maximum energy density, calculated upon the basis of inverse bremsstrahlung, is at the ablation surface) because at the beginning of the pulse, M equals zero. The value μ_c depends on rates alone while μ_L also depends on the integrated mass ablated. Thus, if there is a critical surface in the blowoff, the laser photons encounter it at early time before reaching the plane of maximum energy density by inverse bremsstrahlung absorption. However, if the pulse lasts long enough and constant ablation rate is maintained (by some secondary energy transfer process), then the peak energy density plane will eventually cross the critical surface, preventing most of the remaining incident laser photons from reaching the critical surface. The time t_c at which the crossing occurs can be found by setting $\mu_c = \mu_L$ giving

$$t_c = t_0/\mu_c^2 \quad . \tag{24}$$

Using Eq. 10 in integrating Eq. 20 (replacing Φ_0 by σT^4) from the hot plane at μ_L inward to where $\mu_L = 1$ gives the thermal radiated flux emitted onto the ablation surface as

$$\sigma T^4 \exp(-{}^{R}\kappa_M [1-\mu_L^2]) \quad . \tag{25}$$

Similarly, the thermal radiated flux emitted outward from the hot plane at μ_L is given by

$$\sigma T^4 \exp(-l^R_M \mu_L^2) \quad . \tag{26}$$

The total flux balance for the blowoff is given in Eq. 18 of Ref. 1 but that equation does not include attenuation by the plasma of the laser photons or the thermal radiation. Adding this attenuation, as in Eq. 21 (but with attenuation on the way back out too) and Eq. 26, the total flux balance becomes

$$\{1 - [1-\alpha] \exp(-2 l^L_M)\} \Phi_o = \Phi_a + \exp(-l^R_M \mu_L^2) \sigma T^4 \quad . \tag{27}$$

The new equation, added to the model developed in Ref. 1, is the flux balance at the ablation surface. It is based upon the assumption that a local energy balance at the ablation surface must occur at all times, which basically determines the ablation rate--a very important quantity. That is, the rate of energy flow to the surface from the laser plus that from thermal radiation is set equal to the rate of energy conduction into the target plus the rate of energy consumption to make the transition to the ionized state. No attempt is made at modeling this ablation region in detail; in particular, it is assumed that the temperature of the material jumps from that of the solid (or liquid, not distinguishing which) to that of the ionized blowoff. However, the energy to make this jump should be important and is therefore accounted for with relative accuracy. Combining these assumptions gives the following equation for this energy (actually flux at this stage) balance:

$$\alpha \exp(-l^L_M \mu_L^2) \Phi_o + \exp(-l^R_M [1-\mu_L^2]) \sigma T^4 = \Phi_a \tag{28}$$

where

$$\Phi_a = [\{2/\pi\} K c_p \rho/\tau]^{1/2} T_s + [dm/dt][\Delta H + \{N_o/A\} \Sigma I_Z + \{3/2\} N_o kT/<A>] \quad . \tag{29}$$

The quantity Φ_a is the flux of energy absorbed by the target. In Eqs. 27 and 28, μ_L is a function of time as given in Eq.6 but with M replaced by [dm/dt] t. As indicated above, it should be possible to solve these equations along with the supporting equations above to find dm/dt, and the other parameters of interest, as a function of time. However, in the interest of simplicity, these can be integrated over time if the mass ablation rate and the flux are assumed to be simple functions of time. Assuming these quantities are constant and integrating Eqs. 27 and 28 over time gives the energy balance presented in Eqs.13, 14 and 15. In these equations ε_L, ε_L', ε_i, and ε_o are respectively the attenuation factors for: the laser photons into the ablation surface, the laser photons into and back out from the ablation surface, the thermal radiation from the hot plane in to the ablation surface, and the thermal radiation from the hot plane out of the blowoff.

C. Solution of Equations

The equations for the model are summarized in the Appendix B. These coupled equations are expressed parametrically in terms of T. A consistent solution can be found by iterating on the ionization Z and the blowoff mass M (or the density ρ_o). For example, for a given set of inputs (for some temperature T), two guesses each for Z and M can be selected. Then $<v>$ and ρ can be calculated, which facilitates an iterative solution for Z. Next, the attenuations (ε) can be calculated, followed by evaluation of the two equations for F_o, which will not agree unless the appropriate value for M is used. Finally, the whole procedure can be iterated on M and Z until the appropriate values are found.

III. Calculations with the Model

Results from the model for KrF and CO_2 lasers incident on aluminum, with pulse lengths from 10^{-9} to 10^{-3} s at fluences from the impulse threshold up to over 10^{10} J/m^2 are plotted in Fig.1. Material properties for calculations with the model are given in Appendix C. The ratio of impulse to fluence (impulse coupling coefficient) as a function of fluence is plotted in Figs. 1a and 1b. The same results are replotted versus flux in Figs. 1c and 1d. In Figs. 1e and 1f, part of these results are replotted versus fluence to allow direct comparison of the coupling for KrF (0.25 μm) and

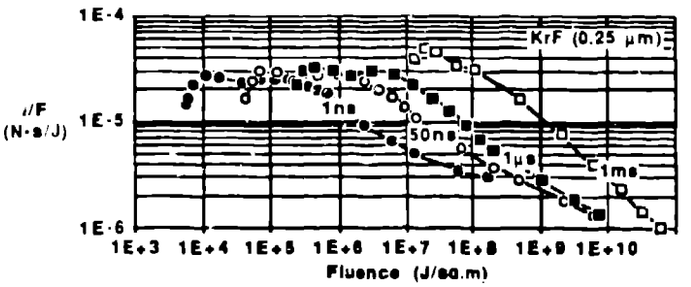

Figure 1a. Coupling versus fluence for KrF.

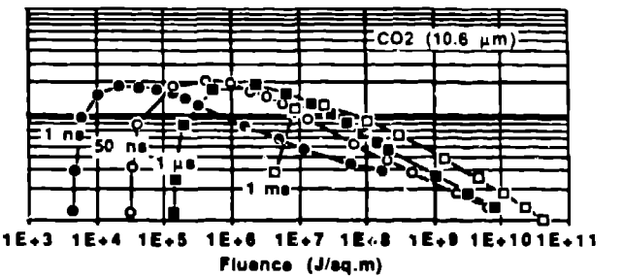

Figure 1b. Coupling versus fluence for CO_2.

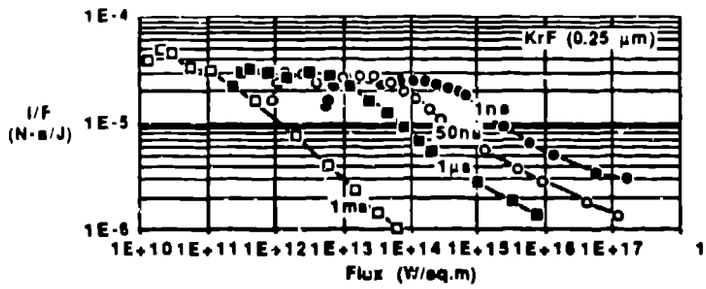

Figure 1c. Coupling versus flux for KrF.

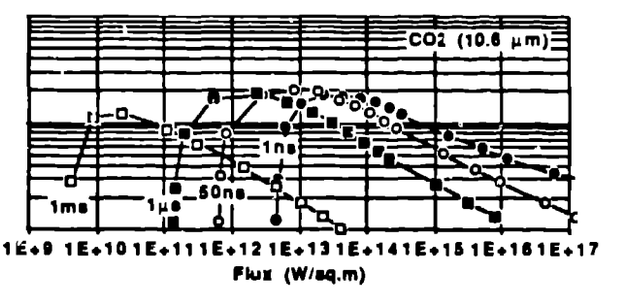

Figure 1d. Coupling versus flux for CO_2.

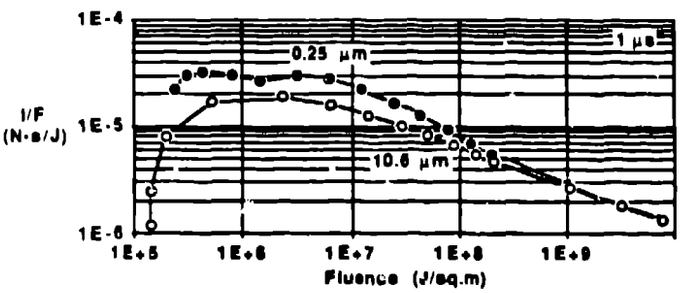

Figure 1e. Coupling versus fluence for 1 μs.

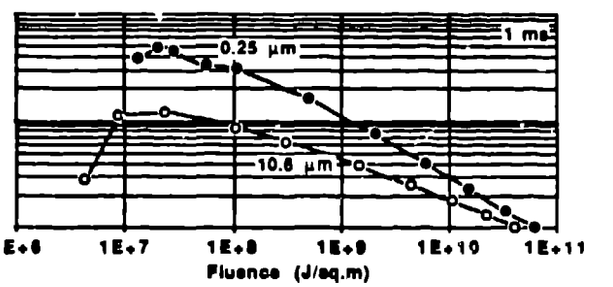

Figure 1f. Coupling versus fluence for 1 ms.

Figure 1. Impulse coupling coefficients versus fluence and flux calculated with the plasma energy balance model for CO_2 (10.6 μm) and KrF (0.25 μm) lasers with pulse widths of 10^{-9}, $50x10^{-9}$, 10^{-6}, and 10^{-3} s normally incident on flat aluminum targets in a vacuum for one dimensional blowoff. These calculations were done with G = 1 and α = 0.5.

CO^2 (10.6 μm) lasers for different pulse lengths. These results show a threshold, a maximum coupling, and a decrease in coupling at high fluence. The mass loss would have to increase in proportion to the fluence to avoid this decrease. If after some point, there was no increase in mass loss with increasing fluence, then the coupling would decrease as the square root of fluence provided the radiation loss into vacuum did not increase with fluence. However, under these conditions radiation losses should increase with fluence causing the coupling to decrease even faster. In some cases, the figures show the coupling decreases about as the square root of fluence (e.g., KrF, 10^{-6} s); this results from some increase in mass loss with fluence as well as some increase in radiation loss with fluence. Figures 1a-1d show that the order of the curves for different pulsewidths reverses when the absessa is switched from fluence to flux (the flux is the fluence divided by the pulse width); in either case, the coupling depends on pulse width. Figures 1e and 1f show that at very high fluences and fluxes the model predicts that the coupling coefficient curves for KrF and CO_2 merge; this is because the plasma is becoming very opaque to photons of both laser wavelengths in this region (so that most of the mass ablation is by secondary energy transfer) making the impulse independent of the laser. When the flux becomes too large, the model becomes invalid because of additional phenomena not included.

Results from the model for aluminum targets are compared with both experimental measurements[7,8,9] and LASNEX computer calculations[10] in Figs. 2 and 3. In Fig. 2a, values for a CO_2 laser (Gemini) with about a 2-ns

pulse width are plotted; the Gemini data are for titanium and various other targets (including organics but not aluminum).[7] Since the data show that the coupling is almost material-independent it seems appropriate to compare the data with model calculations for aluminum, and in fact, Fig. 2a shows good agreement between the model and the data. In Fig. 2b, values are given for the same CO_2 laser (Gemini) modified to have a 1.8-μs pulse length.[8] The comparison with aluminum is within about a factor of 2. LASNEX calculations for Al at high fluence are included in Fig. 2b. These values are a factor of 2 to 3 lower than values from the model. The experimental data, which only exist at a fluence up to the lowest LASNEX fluence, are between the model and LASNEX results.

Figure 3 gives comparisons between measurements and calculations for 50 ns, KrF laser exposure of aluminum and tantalum; the data was taken with the Sprite laser during the Series II experiments.[9] The agreement for aluminum in Fig. 3a between the model (with $\alpha = 0.5$) and the experimental data are reasonably good for fluences below about 10^7 J/m^2. At fluences above 10^7 J/m^2, the experimental data is 2-dimensional because of the small spot size; in this region the measured coupling agrees reasonably well with the 2-D LASNEX runs but is considerably larger than that calculated by either the model or 1-D LASNEX runs. At lower fluence, a substantial fraction of the incident photons are apparently reflected, causing the values calculated with the model with $\alpha = 1$ to give a coupling that is too large; thus the need to use $\alpha = 0.5$. The agreement for tantalum in Fig. 3b between the 1-D data and the plasma-energy-balance-model calculations are good if a value of $\alpha = 0.25$ ($R = 0.75$) is used. Again, 2-D effects in the data cause differences between the measurements and calculations at high fluences.

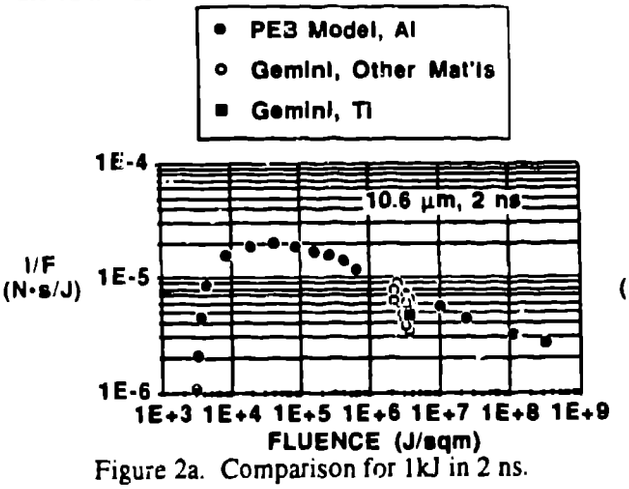

Figure 2a. Comparison for 1kJ in 2 ns.

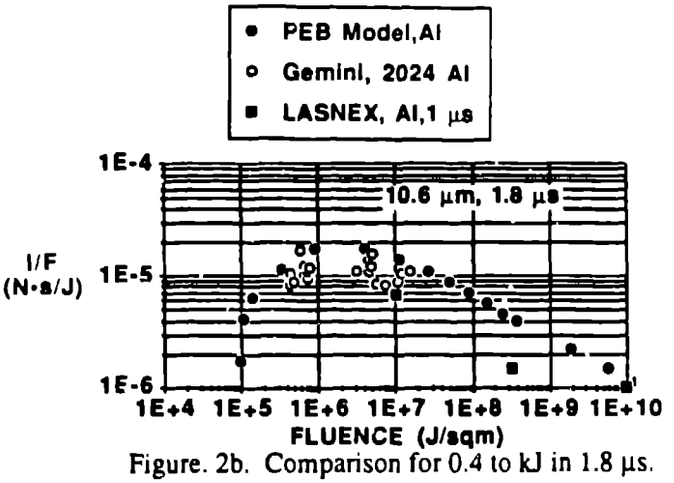

Figure. 2b. Comparison for 0.4 to kJ in 1.8 μs.

Figure 2. Comparison of Gemini laser (CO_2, 10.6 μm) measurements with LASNEX and plasma-energy-balance-model (using $G = \alpha = 1$) calculations for normal incidence on flat targets in a vacuum.

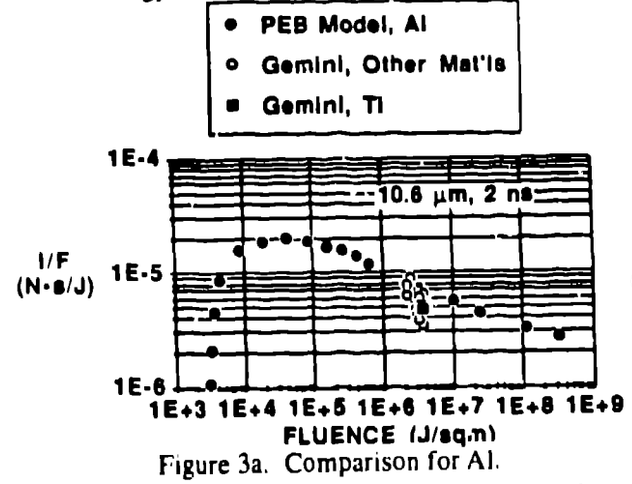

Figure 3a. Comparison for Al.

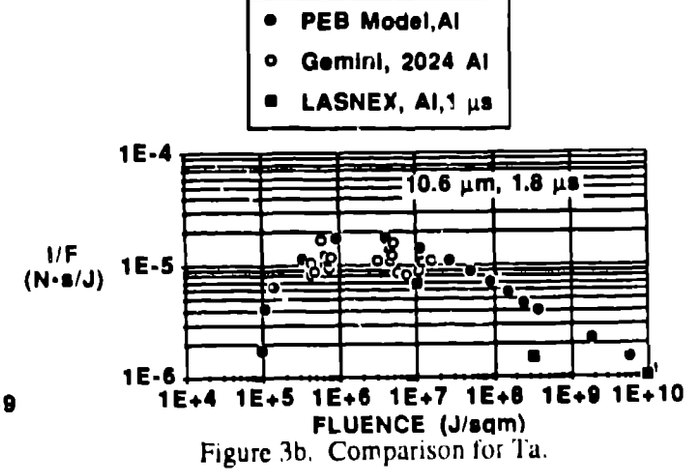

Figure 3b. Comparison for Ta.

Figure 3. Comparison of Sprite laser (KrF, 0.25 μm, 100J, 50 ns), series II measurements with LASNEX and plasma-energy-balance-model (using $G = 1$) calculations for normal incident on flat targets in a vacuum.

Appendix A. Glossary

Material Properties of Target

A = atomic mass

K = thermal conductivity

c_p = specific heat

τ = pulse width

ρ_s = solid density

T_s = sublimation temperature

ΔH = sublimation energy (enthalpy)

I_Z = ionization energy levels

$\langle I_Z \rangle$ = "continuous ionization function"

Laser Properties

R = reflectivity

$h\nu$ = photon energy

ϕ_0 = incident flux (intensity)

F_0 = incident fluence

Other Values

I = impulse = momentum per unit area

T = temperature of blowoff

G = geometric factor

p_0 = pressure at ablation surface

z = linear distance from ablation surface

δ = thermal diffusion distance in target

$\rho = \rho(z)$ = density (mass per unit volume) of blowoff at position z

ρ_0 = density of blowoff at ablation surface

N_0 = Avogadro's number

k = Boltzmann constant

γ = ratio of specific heats

$n_0 = \rho_0 N_0 / A$ = number of atoms per unit volume in blowoff at ablation surface

Z = number of free electrons per atom

$n_{e0} = Z n_0$ = number of free electrons per unit vol in blowoff at ablation surface

n_{ec} = number of free electrons per unit vol at critical surface

$\langle A \rangle = A/[1+Z]$ = average atomic mass per free particle

$\langle v \rangle$ = Average particle velocity for Maxwell-Boltzmann distribution

$z_0 = [\pi/4] \langle v \rangle t$ = average distance particles move during laser pulse

$\zeta = z/z_0$ = scale distance from ablation surface

$m = m(z) = \int_0^z \rho(z')dz'$ = mass (per unit area) depth in blowoff

dm/dt = mass ablation rate

$M = M(t) = m(z=\infty)$ at time t

$M_\tau = M(\tau)$ = total mass ablated

$\mu = 1 - m/M$ = fractional mass thickness of blowoff from outside in to m

μ_L = location of peak laser absorption in terms of μ

z_L = linear position of peak laser absorption

μ_c = location of critical surface in terms of μ

z_c = linear position of peak laser absorption

$\kappa^L = \kappa^L(\mu)$ = (inverse brem.) absorption coefficient for laser photons at μ

κ^L_0 = absorption coefficient for laser photons at ablation surface

l^L_M = mean free path of blowoff to laser photons

ε_L = attenuation of laser photons by blowoff during transit to ablation surface

$\varepsilon_{L'}$ = attenuation of laser photons by blowoff during transit to and from ablation surface

$\alpha' = 1 - (1-\alpha)\,\varepsilon_{L'}$ = fraction of laser fluence F_0 absorbed in target and blowoff

σ = Stefan-Boltzmann constant

$\kappa^R = \kappa^R(\mu)$ = thermal radiation opacity at μ

κ^R_0 = thermal radiation opacity at ablation surface

l^R_M = thermal radiation mean free path of blowoff

l^R_{Li} = thermal radiation mean free path in from μ_L to ablation surface

ε_i = attenuation of thermal radiation in from μ_L to ablation surface

l^R_{Lo} = thermal radiation mean free path out from μ_L to vacuum

ε_o = attenuation of thermal radiation out from μ_L to vacuum

$\xi(\mu)$ = energy density at μ from laser deposition

t_0 = time at which peak energy density leaves ablation surface

t_c = time at which peak energy density crosses critical surface

e = charge of electron

m_e = mass of electron

h = Planck constant

c = speed of light

ν = frequency of laser photons

λ = wavelength of laser photons

Appendix B. Model

Input: $T, G, \alpha, \tau, h\nu, A, K, c_p, \rho_s, T_s, \Delta H, I_Z$

Assume: $\Phi_0 = \text{const.} = F_0/\tau$ for $t \le \tau$; $dm/dt = \text{const.} = M_\tau/\tau$ for $t \le \tau$

$= 0$ for $t > \tau$ $= 0$ for $t > \tau$

Coupled Equations Expressed Parametrically in Terms of T:

$I(\tau) = [1/2]\, G M \langle v \rangle = p_0 \tau$, $p_0 = G n_0 [1 + Z] kT$ for $t \le \tau$,

$I(\infty) = G M \langle v \rangle = G n_0 [1 + Z] kT \exp(-[t-\tau]/\tau)$ for $t > \tau$,

$\langle v \rangle = \{[8/\pi] N_0 kT/\langle A \rangle\}^{1/2}$, $Z = [2/n_0][2\pi m_e kT/h^2]^{3/2} \exp(-\langle I_Z \rangle/kT)$, $n_0 = \rho_0 N_0/A$, $n_{eo} = Z n_0$

$z_0 = [\pi/4] \langle v \rangle \tau$, $\zeta = [z/z_0]$, $\rho/\rho_0 = \exp(-\zeta^2) = 1 - m(z)/M = \mu$, $\rho_0 = [4/\pi][dm/dt]/\langle v \rangle$,

$m(z)/M = \text{erf}(\zeta)$. $m(z) = \int_0^z \rho\, dz'$

$\alpha' F_0 = F_a + \varepsilon_0 \sigma T^4 \tau$, $\varepsilon_L \alpha F_0 + \varepsilon_i \sigma T^4 \tau = F_a$, $\alpha' = 1 - (1-\alpha)\varepsilon_L'$

$F_a = [\{4/\pi\} K c_p \rho \tau]^{1/2} T_s + M[\Delta H + \{N_0/A\} \Sigma I_Z + \{3/2\} N_0 kT/\langle A \rangle]$

$\delta\rho_s = [4 K_i \rho_s \tau / c_p]^{1/2}$, $\gamma - 1 = kT/\{[3/2]kT + [\Sigma I_Z]/[1+Z]\}$,

$\kappa^L{}_0 = [4/3]\{2\pi/[3kT]\}^{1/2}[N_0/A]^2\{\rho Z^3 e^6/[hcm_e{}^{3/2}\nu^3]\}\{1 - \exp(-h\nu/[kT])\}$, $\kappa^L(\mu) = \mu\, \kappa^L{}_0$

$\kappa^R{}_{0,Al}(m^2/kg) = 6 \times 10^4\, T(eV)^{-2}\, \rho(kg/m^3)$ $\kappa^R(\mu) = \mu\, \kappa^R{}_0$

$\mu_L = [\kappa^L{}_0 M]^{-1/2}$ for $[\kappa^L{}_0 M]^{-1/2} \le 1$, $\mu_c = \rho_c/\rho_0 = n_{ec}/n_{eo}$ for $n_{ec}/n_{eo} \le 1$

$= 1$ for $[\kappa^L{}_0 M]^{-1/2} > 1$, $= 1$ for $n_{ec}/n_{eo} > 1$

$t_0 = [\kappa^L{}_0\, dm/dt]^{-1}$, $t_c = t_0/\mu_c{}^2$, $n_{ec} = \pi m_e c^2/(e^2\lambda^2)$

$z_L = z_0 [\ln \mu_L{}^{-1}]^{1/2}$, $z_c = z_0 [\ln \mu_c{}^{-1}]^{1/2}$,

$I^L{}_M = 0.5\, M \kappa^L{}_0$, $I^R{}_M = 0.5\, M \kappa^R{}_0$, $r_{RL} = 0.5\, \kappa^R{}_0/\kappa^L{}_0$

$\varepsilon_L = [1 - \exp(-I^L{}_M)]/I^L{}_M$, $\varepsilon_L' = [1 - \exp(-2\, I^L{}_M)]/[2\, I^L{}_M]$,

$\varepsilon_i = \mu_L{}^2 + [1 - \exp(-I^R{}_M[1-\mu_L{}^2])]/I^R{}_M$, $\varepsilon_0 = \mu_L{}^2 [1 - \exp(-r_{RL})]/r_{RL} + [1-\mu_L{}^2] \exp(-r_{RL})$

Appendix C. Materials properties

Matl	Units	Aluminum	Carbon	Plastic	Tantalum
k	J/[m•s•°K]	2.1E+2	5.9E+1	1.0E-1	5.4E+1
Cp	J/[kg/•K]	9.2E+2	1.3E+3	1.3E+3	1.5E+2
Rs	kg/cu.m	2.7E+3	1.7E+3	1.3E+3	1.7E+4
Ts	°K	2.7E+3	4.1E+3	6.0E+2	5.5E+3
DH	J/kg	1.4E+7	4.5E+7	4.0E+5	5.4E+6
A	atomic mass	26.98	12.01	12.000	180.950
Ion 0	eV	0	0	0	0
Ion 1	eV	5.986	11.260	11.260	7.89
Ion 2	eV	18.829	24.384	24.384	15
Ion 3	eV	28.448	47.888	47.888	23
Ion 4	eV	119.994	64.494	64.494	33
Ion 5	eV	153.72	392.091	392.091	48.27
Ion 6	eV	190.48	490	490	65
Ion 7	eV	241.44			122
Ion 8	eV	284.6			140
Ion 9	eV	330.11			158
Ion10	eV	399.37			177
Ion11	eV	442.08			207
Ion12	eV	2086.05			231
Ion13	eV	2304.11			256
Ion14	eV				289
Ion15	eV				324
Ion16	eV				360
Ion17	eV				387
Ion18	eV				419
Ion19	eV				463

References

1. R. S. Dingus, "Phenomenology of Optical-Laser-Induced Impulse in Vacuo," Los Alamos National Laboratory internal document SDR/U:84-92 (March 8, 1984), to become document LA-10113.

2. J. E. Allen and J. G. Andrews, "A Note on ION Rarefaction Waves," *J. Plasma Physics*, 4, 187-194 (1970).

3. J. E. Crow, P. L. Auer, and J. E. Allen, "The expansion of a Plasma into a Vacuum," *J. Plasma Physics*, 14, part 1, 65-76 (1975).

4. Y. Zel'dovich and Y. Razier, *Physics of Shock Waves and High-Temperature Hydrodynamic Phenomena*, (Academic Press, New York and London, 1966).

5. R. D. Cowan, *The Theory of Atomic Structure and Spectra* (University of California Press, Berkeley, 1981).

6. "SESAME '83: Report on the Los Alamos Equation-of-State Library," Los Alamos National Laboratory document LALP-83-4 (February 1983).

7. R. S. Dingus and D. M. Barrus, "Pulsed Laser Effects--Measurements with the Gemini Laser," Presentation to Directed Energy Effects and Vulneability Workshop (June 1982).

8. W. Z. Osborne, private communication (1984).

9. R. S. Dingus, T. R. King, W. Z. Osborne and C. R. Phipps, Jr., "Single-Pulse Laser Effects Measurements at 248 nm", Los Alamos National Laboratory document, LA-UR 86-1877.

10. S. R. Goldman, G. H. Canavan, R. S. Dingus, and M. A. Mahaffy, "Simulation of the Interaction of Single-Pulsed Optical Lasers with Targets in a Vacuum," in A. S. Kaye and A. C. Walker, (Eds.), *Gas Flow and Chemical Lasers*, 1984 (Adam Hilger, Bristol, 1985), p. 125.